Storm Physics and Lightning Properties over Northern Alabama during DC3

Retha Matthee[1,*], Lawrence Carey[1]
1. Department of Atmospheric Science, University of Alabama in Huntsville, 320 Sparkman Drive, Huntsville, AL 35805, USA.

ABSTRACT: The Deep Convective Clouds and Chemistry (DC3) experiment seeks to examine the relationship between deep moist convection and the production of nitrogen oxides via lightning (LNO_X). In order to accomplish this, flash rate, flash type and areal flash extent need to be analyzed to improve the estimation of LNO_X production in cloud resolving models. Analysis of flash extent over five different domains containing ordinary multicellular convective complexes observed during DC3 over northern Alabama demonstrated that flash extents and flash rates were generally opposed as observed for supercell storms in recent studies. More specifically, the presence of smaller flashes was associated with peaks in the convective surges (seen by increases in flash rates) while larger flashes seemed to be associated with lulls in the convective generator (seen by decreases in flash rates). It is also shown that the total flash extents are highly correlated to the flash rates (Pearson correlation coefficient, $r \geq 0.78$). In addition, it was demonstrated that for the most part, there is negligible difference in r related to whether one bins the flash rates and total extents to a per-minute bin or a radar-bin of ~ 3 to 5 minutes. Finally, it was shown that there is a difference in flash extent between different flash types and that IC-CG Hybrid flashes have an areal extent roughly double that of pure CG flashes; while pure IC flashes have larger areal extents than pure CG flashes.

INTRODUCTION

The Deep Convective Clouds and Chemistry (DC3) experiment occurred during May and June 2012 and was an interdisciplinary study with the goal to investigate and understand the relationship between the microphysical, kinematic, and electrical properties of deep moist convection (DMC) [Barth et al. 2013]. Specifically, the DC3 experiment seeks to examine the relationship between DMC and the production of nitrogen oxides (NO_X) via lightning (LNO_X). In order to accomplish this, storm microphysical and kinematic information from radar was compared to flash rate, flash type and areal flash extent to improve the estimation of LNO_X production in cloud resolving models. The focus of this study therefore will be to examine lightning properties of DMC across northern Alabama (NA) during the DC3 campaign through use of polarimetric radar [UAHuntsville's Advanced Radar for Meteorological and Operational Radar (ARMOR)], and lightning mapping [using the North Alabama Lightning Mapping Array (NALMA) and Vaisala National Lightning Detection Network™ (NLDN)] platforms. Specifically,

* Contact information: Retha Matthee, Department of Atmospheric Science, University of Alabama in Huntsville, Dept. of Atmospheric Science, University of Alabama-Huntsville, 320 Sparkman Drive, Huntsville, AL 35805, USA, retha.matthee@nsstc.uah.edu.

ARMOR, NALMA and NLDN are being used to explore the relationship between radar inferred microphysical (e.g., ice mass) measurements to flash typing [e.g. inter-cloud (IC) and cloud-to-ground (CG) lightning] and flash area/extent.

BACKGROUND

Cloud electrification and lightning is an important phenomenon that plays a pivotal role in the production of NO_X, however, there is considerable variability in the estimates of LNO_X [Wang et al. 1998; Schumann and Huntrieser, 2007; Koshak et al. 2014]. In addition, there is some controversy as to whether the lightning type (e.g. cloud−to−ground [CG] or intra−cloud [IC]) has any influence on the amount of NO_X generated per flash. Barthe and Barth [2008] provide a list of studies that examine this aspect of NO_X production using two different approaches (amongst others). The first approach uses an explicit electrical scheme [e.g. Zang et al. 2003 and Barthe et al. 2007]; while the second approach uses the parameterization of LNO_X [e.g. Pickering et al. 1998; DeCaria et al. 2000, 2005 and Ott et al. 2007]. Some modeling studies of NO_X suggest that there is roughly an order of magnitude difference in NO_X production between CG and IC lightning [Price et al. 1997; Pickering et al. 1998; Dye et al. 2000]. Price et al. [1997] state that CG flashes produce more NO_X than IC flashes based on the stronger energetics associated with CG's; while Pickering et al. [1998] states that simulated CG flashes produced larger *instantaneous* NO_X values versus IC flashes. Output from the NASA Lightning Nitrogen Oxides Model (LNOM) suggests that the amount of NO_X produced per CG flash is roughly an order of magnitude greater than the amount of NO_X produced per IC flash [Koshak et al., 2014]. However, in a study by Dye et al. [2000], it was shown that IC flashes were the more significant contributor to NO_X (at least for their specific study); while Barthe and Barth [2008] performed sensitivity studies, which showed that varying the IC:CG ratio yielded very little difference in the LNO_X profile.

In addition to flash type possibly being important in the modeling of NO_X produced by lightning, other scientists argue that areal flash length [Wang et al. 1998 and Barthe and Barth, 2008] as well as flash multiplicity [Wang et al. 1998] may also be important. Furthermore, Carey et al. [2005]; Dye and Willett [2007]; Hodapp et al. [2008]; Ely et al. [2008]; Bruning and MacGorman [2013] and Calhoun et al. [2013] showed in one way or another that flashes that developed within the convective core and updraft region of mesoscale convective systems [MCSs] and supercells occurred more frequently, but with smaller areal extents as compared to flashes that developed further away from or behind the convective core (i.e. in the stratiform region of mesoscale MCS or anvils of supercells), which were less frequent but larger in areal extent. Most of these studies either focused on supercells or MCSs and with the exception of Bruning and MacGorman [2013], the flash rate versus flash extent anti-correlation were found inadvertently while examining other features of these storm types. Bruning and MacGorman [2013] recently presented a theoretical argument to explain these observations, which they also demonstrated in two supercells. They stated that frequent breakdown and large flash extents are opposed and that the kinematic and electrical properties of the storm suggested that advection of precipitation that is charged, couples the electrical and kinematic properties of a thunderstorm [Bruning and MacGorman 2013].

Due to these different findings and the fact that cloud-resolving models use parameterization schemes for lightning-produced NO_X that make various assumptions, it is necessary to verify whether flash typing and areal flash extent is important in the LNO_X parameterization schemes. As such, this

paper will focus on one storm complex (comprised of five different domains) that occurred on 21 May 2012 in NA during the DC3 campaign and explicitly analyse the flash extents over a period of time, as well as compare the flash extents between different flash types. This study closely follows the work by Bain et al. [2013], Carey et al. [2013], Matthee et al. [2013] and Carey et al. [2014], all of which showed the microphysical and kinematic properties of one of the storm domains that will be presented here.

DATA AND METHODOLOGY

DC3 took place in May – June 2012 over NA and two other locations (Colorado and Oklahoma/Texas) [Barth et al. 2013]. For DC3 Alabama, the Advanced Radar for Meteorological and Operational Research (ARMOR) [Petersen et al. 2005] and the Weather Surveillance Radar - 1988 Doppler (WSR-88D) comprises the dual-Doppler and dual-polarization radar network (Figure 1). Although not used in this analysis, the S-band WSR-88D is operated and owned by the National Weather Service (NWS) and is located at Hytop, AL (KHTX). The C-band ARMOR radar is located at the Huntsville International Airport and is co-owned by the University of Alabama in Huntsville (UAH) and WHNT. The C-band ARMOR radar, in conjunction with the NALMA and NLDN lightning networks were used extensively in this and related research. ARMOR has a beamwidth of 1° and operates in a simultaneous transmit and receive of both the horizontal and vertical channels. Additional specifications of ARMOR are discussed in Petersen et al. [2005]. NALMA is owned and operated by NASA MSFC. The network consists of 11 very high frequency (VHF) antennas across northern AL that detect radiation emissions from propagating leaders associated with lightning using a time-of-arrival technique [Goodman et al. 2005]. The NALMA in conjunction with the NLDN allow for a detailed depiction of total lightning.

Both ARMOR and KHTX radar data underwent a vigorous quality control process implemented at UAH. As a result of ARMOR`s relatively shorter wave length (relative to KHTX), propagation effects occur with the presence of heavy rain. To address this issue, all raw ARMOR data were corrected for attenuation and differential attenuation using a self-consistency method outlined in Bringi et al. [2001]. The corrected ARMOR and raw KHTX radar data were then manually inspected using the National Center for Atmospheric Research`s (NCAR) SOLO radar visualization and editing software. During this labor-intensive process, aliased Doppler velocities were corrected and spurious echoes associated with second trip echoes, ground targets and anomalous propagation were removed. In the event that ARMOR operations consisted of sector volumes, an internal method for correcting any azimuth pointing angle error was employed. Once the quality control of ARMOR and KHTX data was completed, both sets of data were gridded using NCAR`s REORDER package [Mohr et al. 1986]. Polarimetric and Doppler radar quantities were gridded from radar space to a Cartesian grid with spacing of 1 km in x, y and z using the Cressman Weighting scheme [Cressman 1959].

Although not discussed here, precipitation ice and graupel mass and volume, as well as various updraft calculations, were done for the -10 °C to -40 °C charging region in order to obtain when the storm complexes were in their developing, mature and dissipating phases, as previous studies have shown that locations of graupel, hail and ice crystals can be utilized to locate areas of lightning [Doviak and Zrnić 1993; Hondl and Eilts 1994; Carey and Rutledge 1996; Carey and Rutledge 2000; Straka et al. 2000; Carey et al. 2003; Wang and Carey 2005; Lund et al. 2009; to name but a few]. Carey and Rutledge [2000] showed that precipitation ice and water in the mixed–phase (or charging) region are strongly

correlated to lightning. Further, increased updraft strength inferred from radar variables directly resulted in more ice mass aloft, and thus more lightning [Carey and Rutledge 1996]. Refer to Bain [2013], Bain et al. [2013], Matthee et al. [2013] and Carey et al. [2014] for discussions on these ice masses, volumes, as well as updraft strength calculations which are applicable to the storms discussed here. In addition to these precipitation ice and graupel calculations, the volume of particles with horizontal reflectivity (Z_H) > 10 dBZ at temperatures colder than -40 °C was also calculated. It is important to note that Z_H up to 40 DBZ was reached at times above the freezing level (-40 °C) and as such, it was decided to not call these ice volumes "non-precipitating" ice volumes, because these may very well have been precipitating and thus we refer to these ice volumes as "ice aloft" and will be presented herein.

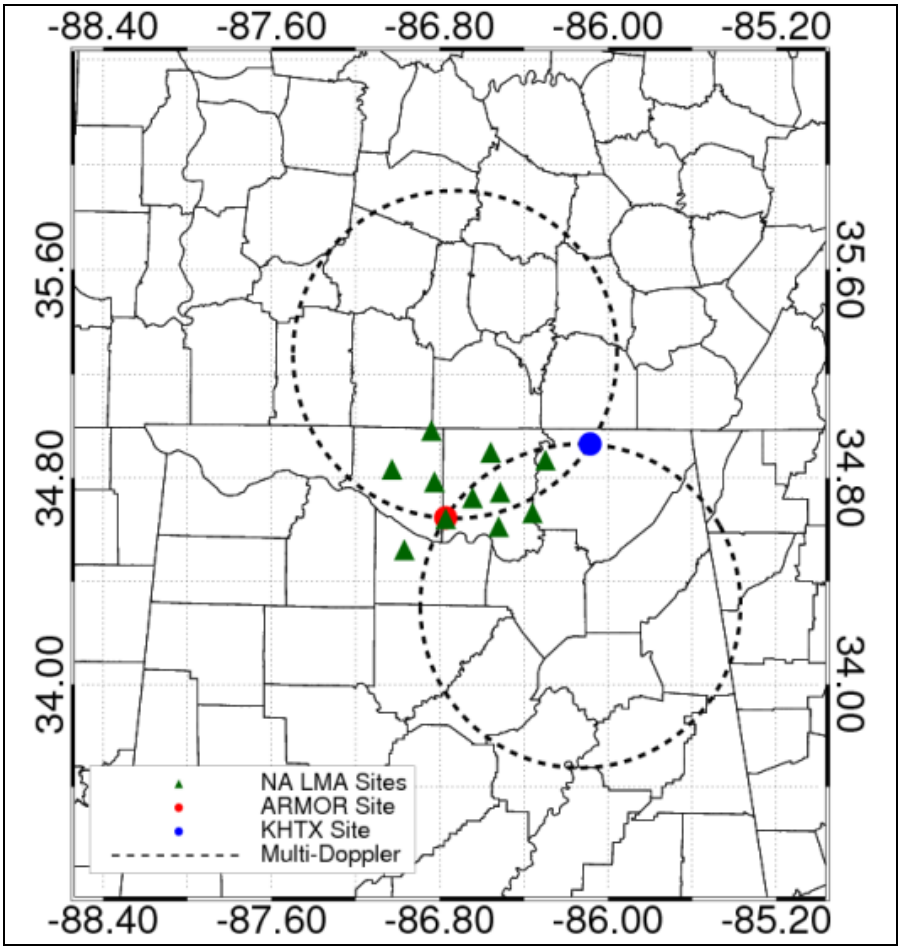

FIGURE 1: A map of the DC3 Alabama domain. The green triangles represent NALMA VHF antennas. The solid red dot represents the location of the ARMOR radar. The solid blue dot represents the location of KHTX. The short-dashed lines represent regions where multi-Doppler wind synthesis can be performed.

The individual NALMA VHF radiation sources were clustered into a lightning flash, based on spatial and temporal criteria outlined in Thomas et al. [2003]. A minimum of 10 VHF sources is required in order for it to be classified and used as an individual flash in an attempt to remove erroneous VHF radiation

sources, such as noise. For the flash rate calculations, the first VHF source of each flash was used as the flash initiation point. Each flash is then counted, either over a given radar volume (radar volume time is defined as the time between each successive radar volume; roughly 3 to 5 minutes per bin) when the actual flash extents are compared, or the flashes are counted over one minute and compared to the total flash extent (all flash extents in each one minute time bin are added together to form the total flash extent per one minute time bin). The flash extent or length scale was calculated as the square root of the horizontal convex hull (or polygon) area surrounding the NALMA VHF sources in the horizontal for each flash [see Fig. 2, as explained in Bruning and MacGorman, 2013]. The flashes are binned according to the radar volume time in order to compare the flash rates to the radar-derived ice and graupel masses and volumes as well as the updraft speeds.

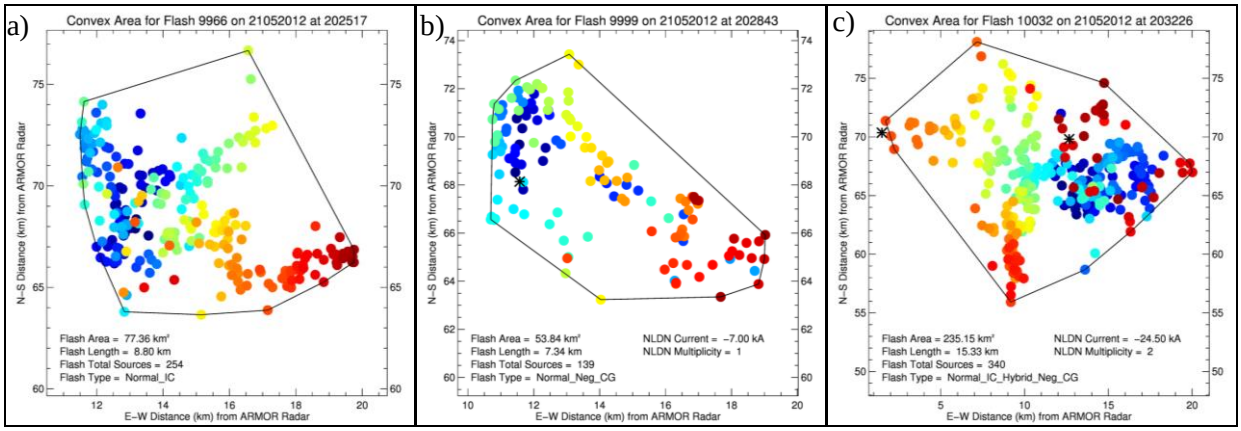

FIGURE 2: Images showing how the convex hull area is calculated through the convex hull (polygon) method; (a) is an example of an IC, (b) an example of a CG and (c) is an example of an IC-CG Hybrid flash [Following Bruning and MacGorman, 2013]. The black star indicates the NLDN event location. The colored circles are each source location constituting a flash, color-coded according to first source (dark blue) to last source (dark red).

As part of the flash clustering algorithm, each flash is also classified per flash type. There are 11 flash types: 1) Normal Negative CG; 2) Normal Positive CG; 3) Unclassified Negative CG; 4) Unclassified Positive CG; 5) Normal IC; 6) Inverted IC; 7) Unclassified IC; 8) Normal IC-CG Hybrid Negative CG; 9) Normal IC-CG Hybrid Positive CG; 10) Low Flash; and 11) Unclassified Flash. For the overall flash results as well as the flash rate per minute calculations, all flash types were used and no distinction was made between the various flash types. However, for the IC, CG and IC-CG Hybrid specific comparisons, only flashes that were unambiguously classified (as in Table 1) were used in the analysis. The reason for only using unambiguously classified flashes is because many LNO_X modeling studies distinguish between IC and CG flashes and state that CG flashes produce more NO_X than IC flashes. However, no such study exists on which type of lightning has a larger flash extent. If the flash length/extent is indeed important in the calculation of LNO_X, as suggested by Wang et al. [1998] and Barthe and Barth [2008], then it is important to analyze the flash extents between IC and CG flashes. Therefore, in order to not bias the results, all unambiguously classified flashes were removed from the

flash dataset used to compare the IC, CG and IC-CG Hybrid flash extents.

It is important to note that although "Normal Positive CG" and "Normal IC-CG Hybrid Positive CG" are used in the flash typing, no positive CG flashes occurred over any of the storm domains discussed here. In addition, Normal Negative (Positive) CG flashes are those that consisted of VHF sources with low altitudes (~ < 6 km) and a negative (positive) NLDN CG event occurring at the same location and time interval. Normal and Inverted IC flashes have VHF sources that occur at high altitude (~ > 6 km) with either positive or negative initial velocity, respectively, while no NLDN CG event occurred. Finally, IC-CG Hybrid flashes is essentially a hybrid between IC and CG flashes and occurs when the VHF sources start at a high altitude (~ > 6 km) and has either a positive or negative NLDN CG event at the same location and time interval. Other research, such as that done by Lu et al. [2012]; Lang et al. [2013] and Qie et al. [2013] also differentiated between IC, CG and IC-CG Hybrid flashes and more details about these classification types can be found in these papers.

TABLE 1: Indicating how the flash types were grouped for the specific flash typing analysis.

Flash Type	**Classified Flash**
CG	Normal Negative CG
	Normal Positive CG
IC	Normal IC
	Inverted IC
IC-CG Hybrid	Normal IC-CG Hybrid Negative CG
	Normal IC-CG Hybrid Positive CG

Finally, storm identification and tracking was done by a human expert on a subjective basis. As is usual for NA, there were multiple storm complexes that occurred on 21 May 2012. These storm complexes merged and separated from other storm complexes. As such, it was decided to create multiple storm domains (ranging from a small multicellular complex to a large domain incorporating various different storm cells and complexes). These domains are shown in Figures 3 – 5. The box colors in these Figures indicate the following: Purple is Domain A; Orange is Domain B; Blue is Domain C; Green is Domain D; and Red is Domain E. The storms in Domain A and B merge with each other as well as another multi-cellular complex at ~ 21:04 UTC which eventually forms a line of convective storms, as in Figure 5 and Table 2. One of the main reasons for various analysis domains is to verify if the flash rate versus flash extent results vary whether one focuses on a single storm complex, or over a large domain covering ~ 10,000 km^2 as well as if the flash extent per flash type vary as a result of domain. If the results do not vary, then it would be possible in future analysis of similar research to save time by not tracking individual storm clusters and just use a large domain for analysis purposes.

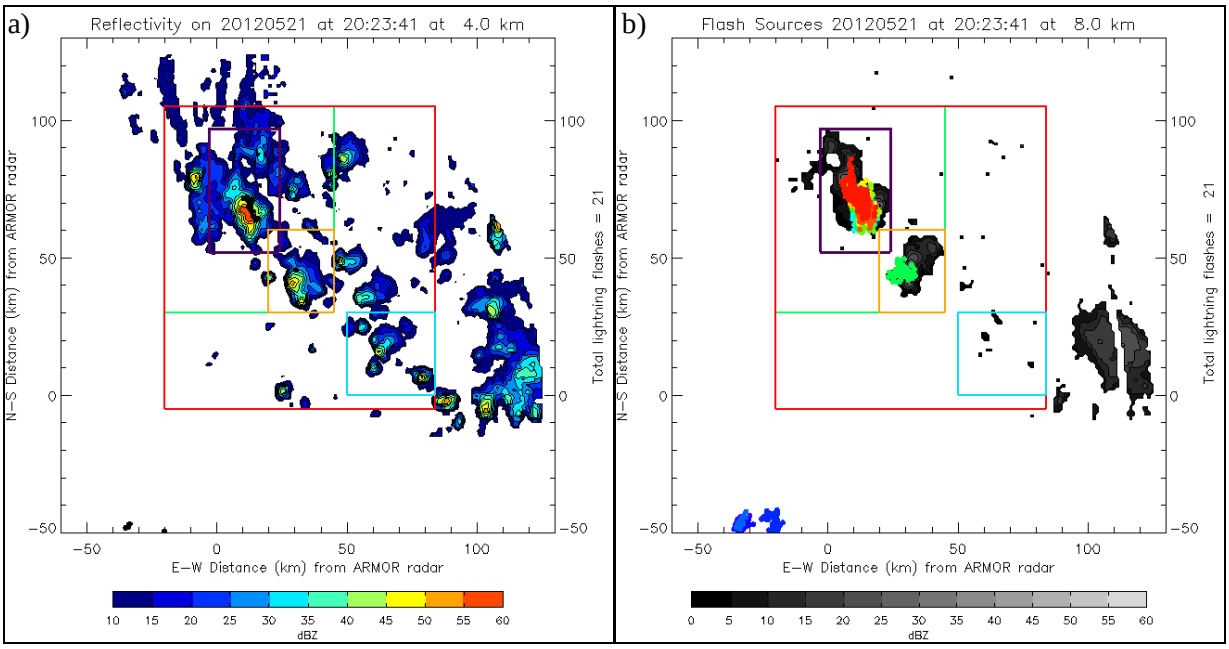

FIGURE 3: Horizontal reflectivity (Z_H) at 20:23 UTC showing the various tracking domains at (a) 4 km and (b) 8 km vertical height. In (a) the Z_H is seen in color (from 10 dBZ [dark blue] to 60 dBZ [red]); while the flash initiation point is shown in a black circle. In (b) the Z_H is in grey-levels (from 0 dBZ [black] to 60 dBZ [light grey]); while the sources for each flash is color-coded according to first flash (blue) and last flash (red) during the radar time interval. In both (a) and (b) the box colors indicate the following: Purple = Domain A; Orange = Domain B; Blue = Domain C; Green = Domain D; and Red = Domain E.

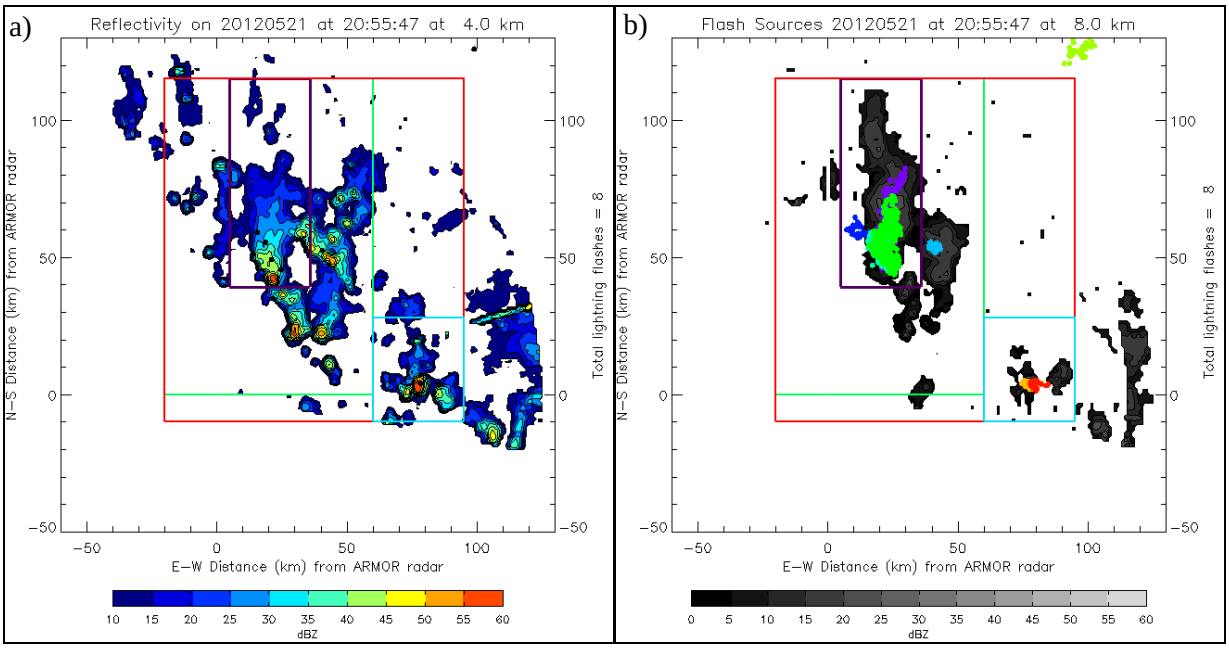

FIGURE 4: Same as Figure 3, but at 20:55 UTC.

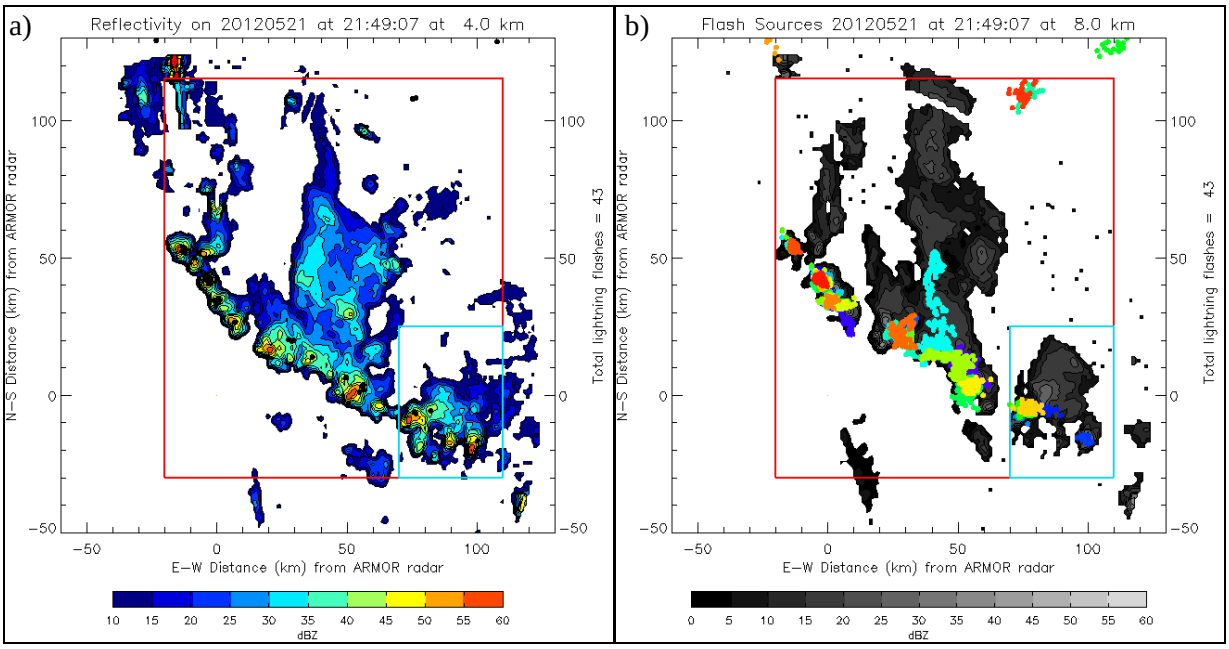

FIGURE 5: Same as Figure 3, but at 21:49 UTC.

TABLE 2: Showing the tracked time, total flashes and highest flash rates (per minute and radar time) for each domain.

	Track Start Time	**Track End Time**	**Total Tracked Time**	**Domain Clarification**	**Total Flashes over Tracked Time**	**Highest Flash Rate per Minute**	**Highest Flash Rate per Radar Time**
Domain A	20:06	21:04	58 min	Merged with Domain B	102	6	15
Domain B	19:55	20:32	37 min	Merged with Domain A	24	2	4
Domain C	20:51	21:53	62 min	Never merged with any other Domain	66	2	7
Domain D	19:35	21:44	129 min	Consisted of Domain A and B	296	8	26
Domain E	19:35	21:53	138 min	Consisted of Domain A, B and C	437	13	40

RESULTS AND DISCUSSION

As mentioned earlier, although not shown here, previous studies have shown that an increase in updraft speed as well as ice and graupel mass and volumes are directly related to an increase in flash rates [Carey and Rutledge, 1996, 2000; Wiens et al. 2005; Deierling et al. 2008; to name a few]. In addition, Bain et al. [2013]; Bain [2013]; Matthee et al. [2013] and Carey et al. [2014] showed that the updraft

speed and ice/graupel mass and volumes were correlated to flash rates for domain 1 in Figures 3-5. Therefore, only the flash rates, flash extents and ice volumes at temperatures < -40 °C, as these evolved over time, will be included in this analysis.

Flash count versus flash extent

The NALMA flash count per radar time and associated flash extents, calculated from the square root of the convex hull area surrounding the VHF sources in the horizontal [Bruning and MacGorman 2013], is provided in Figures 6 – 10. It is important to note that for these calculations, all flash types were used and no distinction was made between IC, CG or IC-CG Hybrid flashes (including all other types of flashes). In general, the flash extent lagged the flash rate and other measures of convective vigor. For example, the NALMA flash extent increased rapidly *after* the storms became more convectively vigorous, i.e. after 20:23 UTC for Domain A, D and E (Figs. 6, 9 and 10), as indicated by the peaks in total flash rate.

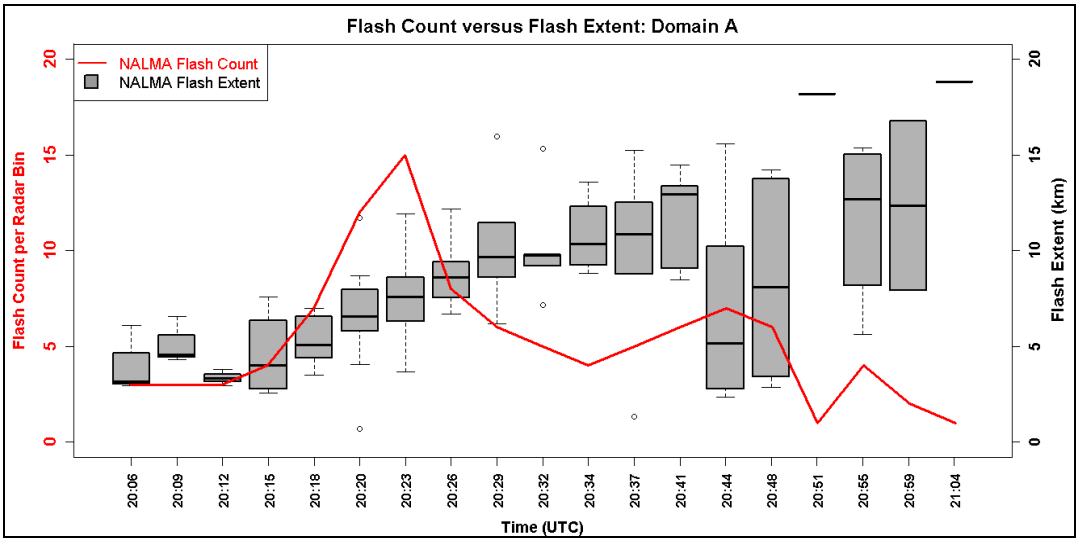

FIGURE 6: Evolution of the NALMA flash count (per radar time) represented by the red solid line and flash extent (km) represented by the grey box for domain A. The grey box represents the interquartile range (IQR; 25–75%) of the flash extent while the horizontal line that divides the box into two sections is the median value. The upper whisker is the (75th percentile + 1.5xIQR), or upper inner fence, and the lower whisker is the (25th percentile - 1.5xIQR), or lower inner fence [Wilks, 2006]. Any values larger (smaller) than the upper (lower) whisker are seen as outliers and are shown as circles. When there is only 1 flash in the timeframe, it is represented by a black horizontal line.

After the convective surge weakened (shown by a decrease in the flash rates), the median flash extent continued to increase and then plateaued and the overall distribution of the flash extent greatly broadened (i.e., there were both small and large flashes present after the convective surge). Stronger convective surges, characterized by relative maxima in flash rate, were associated with corresponding temporary decreases in the median flash extent, for example, after 21:31 UTC in Figures 9 and 10. More

specifically, the presence of smaller flashes was associated with peaks in the convective generator while larger flashes seemed to be associated with lulls in the convective generator after large swaths of ice aloft had been produced. This is especially true in Domains A, B, D and E. The reason for Domain C (Fig. 8) not showing the same results might be because the storm was only tracked for a total of ~ 1 hour and was in its mature phase when tracking stopped due to the storm moving out of the radar domain. However, at the time of highest flash rates (i.e. at 21:23 UTC) the flash extents are smallest, and increases systematically as the flash rates slowly decreases (Fig. 8).

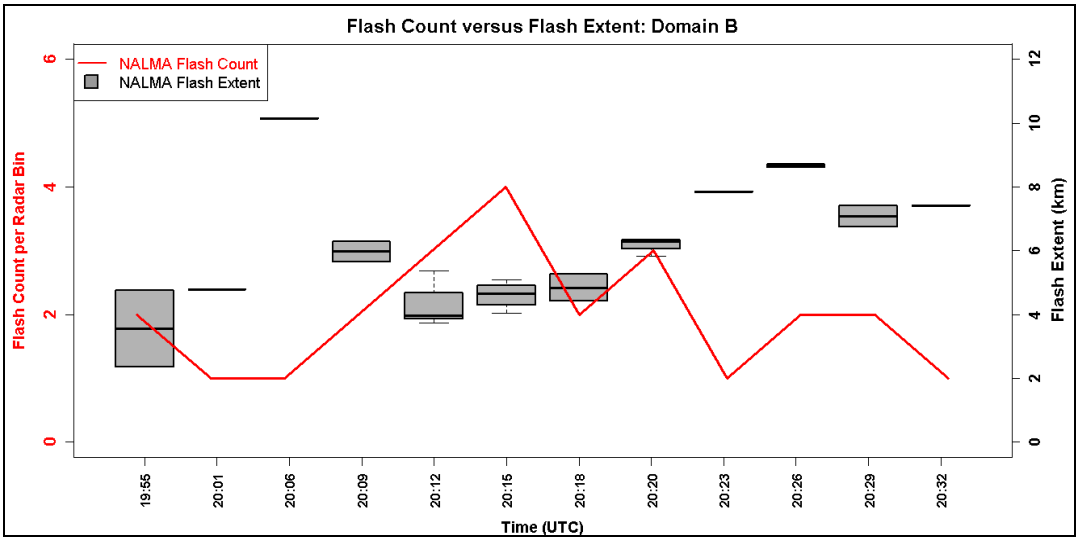

FIGURE 7: Same as Figure 6, but for domain B.

Again, the reasoning behind the multiple storm domains were to confirm if the flash rate versus flash extent results vary whether one focuses on a single storm complex, or over a large domain covering ~ 10,000 km^2 as well as if the flash extent per flash type vary as a result of domain. Overall, the flash extent and flash rate in these multicellular domains were generally opposed as observed by Bruning and MacGorman [2013] for supercell storms. In addition, other research have shown that flashes in the stratiform regions of MCSs and anvil regions of supercell storms are more horizontally extensive and layered as compared to flashes in the convective regions [Carey et al., 2005; Dye and Willett, 2007; Hodapp et al., 2008; Ely et al., 2008; Bruning and MacGorman, 2013 and Calhoun et al., 2013]. More specifically, Dye and Willet [2007] stated that after the convective core had ceased, the charge structure in long-lived Florida anvils became more uniformly layered, and horizontally extensive. These horizontally layered charge regions need more charge to create electric field magnitudes large enough for breakdown to occur [Bruning and MacGorman, 2013]. This implies that uniformly layered and horizontally extensive charge regions have fewer opportunities for breakdown to occur, and therefore lower flash rates, but larger (or more extensive) flashes occurring. On the other hand, when the storms are going through convective surges (i.e. when updraft speeds and graupel/ice mass and volumes are increasing) there exist pockets of charge over the storm complex that requires less charge to create electric field magnitudes large enough for breakdown to occur [Bruning and MacGorman, 2013]. Therefore higher flash rates with smaller flash extents occur during the convective surge of storms, and

smaller flash rates with larger flash extents occur after the convective surges, or when the storm complexes are entering the dissipating phases, as seen in Figures 6 – 10.

We also see that, for the most part, analyzing various domains lead to the same result: Flash extent and flash rate in these multicellular domains are generally opposed and this is independent of storm domain. However, one should be cautious when using this result, as all of the numerous cells included in these analysis domains were going through their developing, maturing and dissipating phases at roughly the same time. Therefore these findings (that flash extent is opposed to flash rates over any domain) might not be applicable when there are multiple convective cells that are in *different* times of their lifecycles.

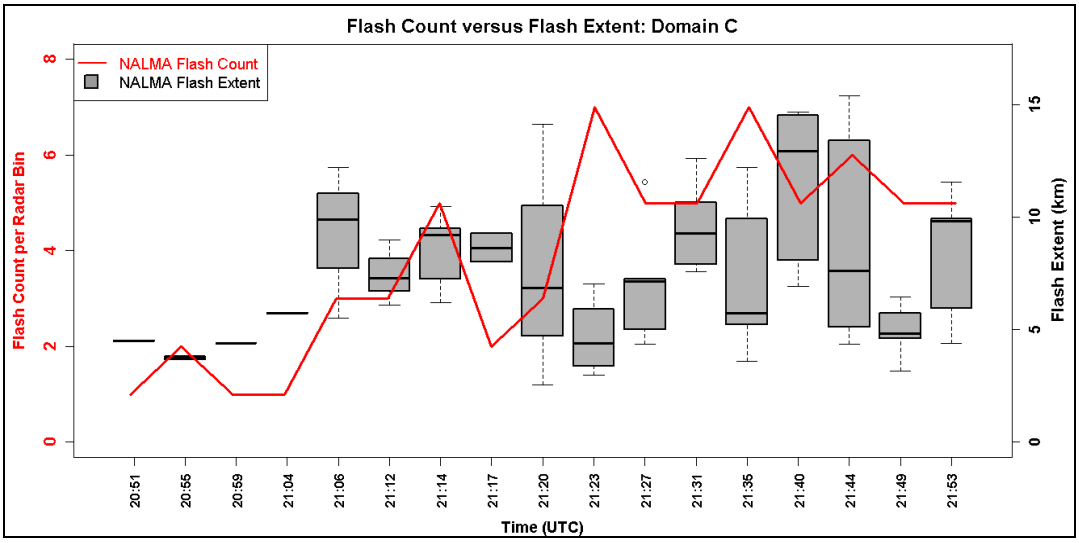

FIGURE 8: Same as Figure 6, but for domain C.

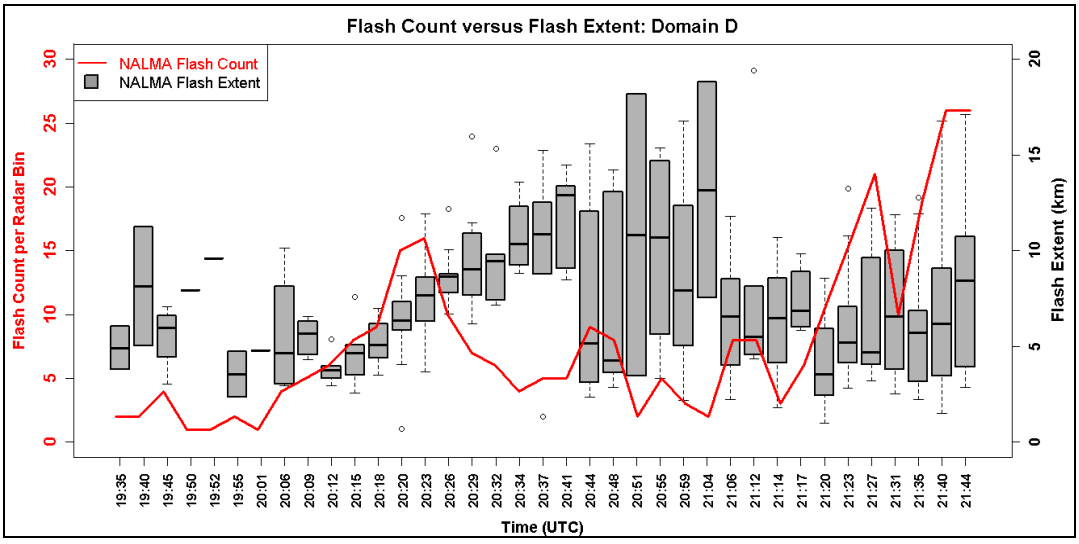

FIGURE 9: Same as Figure 6, but for domain D.

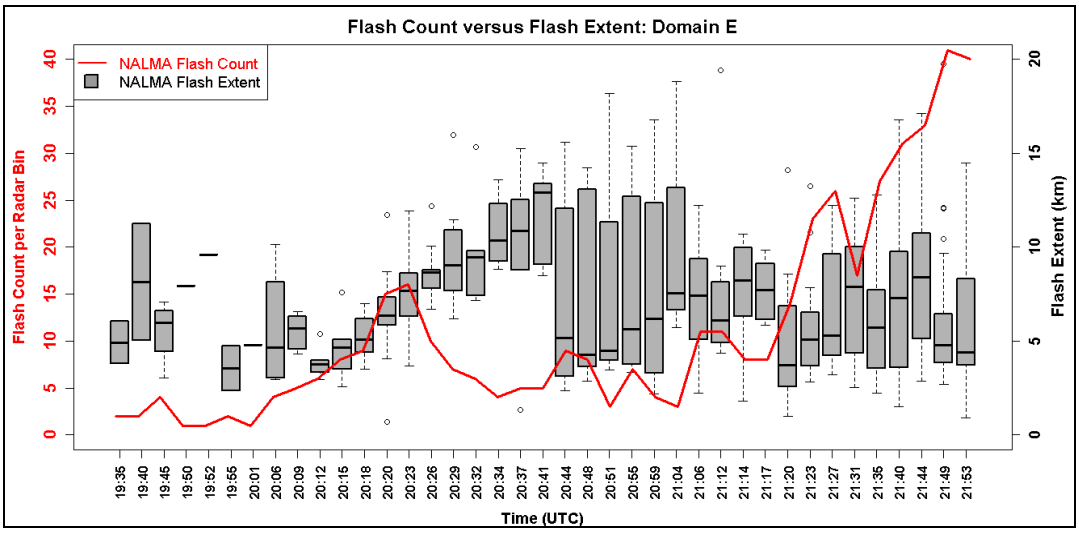

FIGURE 10: Same as Figure 6, but for domain E.

Ice Volumes at temperatures < -40 °C versus flash extent

Based on the finding that convective surges in the charging zone (-10 °C to -40 °C layer) preceded flash extent, the ice volume aloft ,or in and near the top of the convection in the various domains, were calculated for Z_H > 10 dBZ and T < -40 °C. These ice volumes were compared to the flash extents per radar bin and can be seen in Figures 11 – 15. For the most part, the flash extents increase as the ice volumes increased and thus the ice volume trend aloft was well correlated with the overall trend in the median flash extent.

Looking at Figure 11 (domain A), for example, both the flash extent and the ice volume increased between 20:12 and 20:29 UTC and then plateaued with minor oscillations for the next ~ 35 minutes. Domain B (Fig. 12) also showed an increase in both flash extent and ice volume between 20:12 and 20:29 UTC, after which both properties decreased. Domain C (Fig. 13) on the other hand, did not show as strong of a correlation between flash extents and ice volume, but this could again be due to the storm only being tracked for a total of ~ 1 hour and was in its mature phase when tracking stopped due to the storm moving out of the radar domain. This could therefore lead to inconsistencies, as the same irregularities were observed in the flash count per radar bin versus the flash extent results in Figure 8. In addition, during the tracking-phase, the storm had fairly low flash rates, with a maximum of 2 flashes min^{-1}. However, there does seem to be some correlation between the two properties, especially between 21:20 and 21:44 UTC.

Domains D and E (Figs. 14 and 15 respectively) were again the domains that included larger areas and were tracked over longer time periods. For these two domains, there is good correlation between the flash extent and ice volume aloft, as both properties increase between 20:12 and ~ 21:04 UTC. The initial variability of the flash extents that occur during smaller volumes of ice aloft before 20:12 UTC could be smaller storm cells that never really developed much vertically, but did develop enough graupel and precipitation ice in the charging region to produce lightning. After 21:04 UTC, there is some variability in both the ice volumes aloft and the flash extents for both domains, but generally, as the median flash extents increase (decrease) the ice volume aloft increases (decreases). However, it is clear that there exists

some degree of variability, especially during the initial and final stages of tracking, as can be seen by the wide range of Pearson Correlation Coefficient (r) values in Table 3. It seems that when only a single multicellular storm is tracked (i.e. Domain A) the r values are higher when the ice volume aloft is compared to the median and maximum flash extent per radar time. On the other hand, when larger domains are tracked, such as Domains D and E, it seems that the r value is higher when comparing the maximum and total (when all flash extents are added together for each radar bin) flash extents to the ice volume aloft. This could be related to the amount of charge available in these ice volumes, which would directly impact the flash extents. It is clear that more analysis is needed with regards to what specifically controls the flash extents. Is it the small, medium or large ice aloft, or possibly a combination of these sizes? Could small ice in the charging zone be more related to flash extents? In addition, these types of questions need to be answered for a variety of storms occurring in different environments. Dye and Willet [2007] observed horizontally extensive electric field magnitudes > 10 kVm^{-1} in long-lived anvils where Z_H > 20 dBZ. This indicates that there is charge in these anvils, and these horizontally extensive charge layers may have an important impact on the flash extent during the mature and dissipating phases of thunderstorms of all types. As such, further analysis will be done using the Dye and Willet [2007] reflectivity value for the anvil areas specifically, thereby including warmer temperatures, and not just T < -40 °C. Another reason for following the Dye and Willet [2007] method in future, is because as the storm evolves, the anvil, and especially Z_H > 10 dBZ at T < -40°C gradually expands, while the flash extents will decrease due to the amount of charge available for breakdown decreasing. This can be seen for Domain D (Fig. 14) and Domain E (Fig. 15) after 21:04 UTC. In addition, it seems that tracking of individual storm cells or clusters are important, and when one combines various storm cells into a larger domain, the flash extent versus ice volume aloft comparison breaks down. Thus it is best to track these storms separately and not group them all together when doing these types of ice volume comparisons.

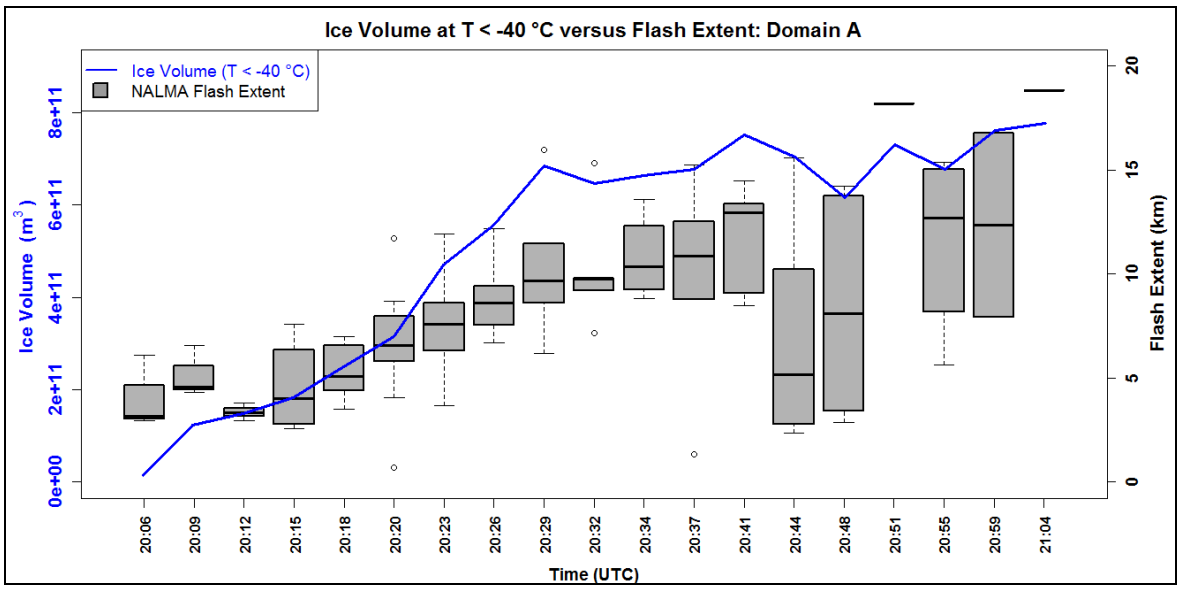

FIGURE 11: Evolution of the ARMOR ice volume at temperatures colder than -40 °C (per radar time) represented by the blue solid line and flash extent (km) represented by the grey box for domain A. See Figure 6 for explanation on the box plots.

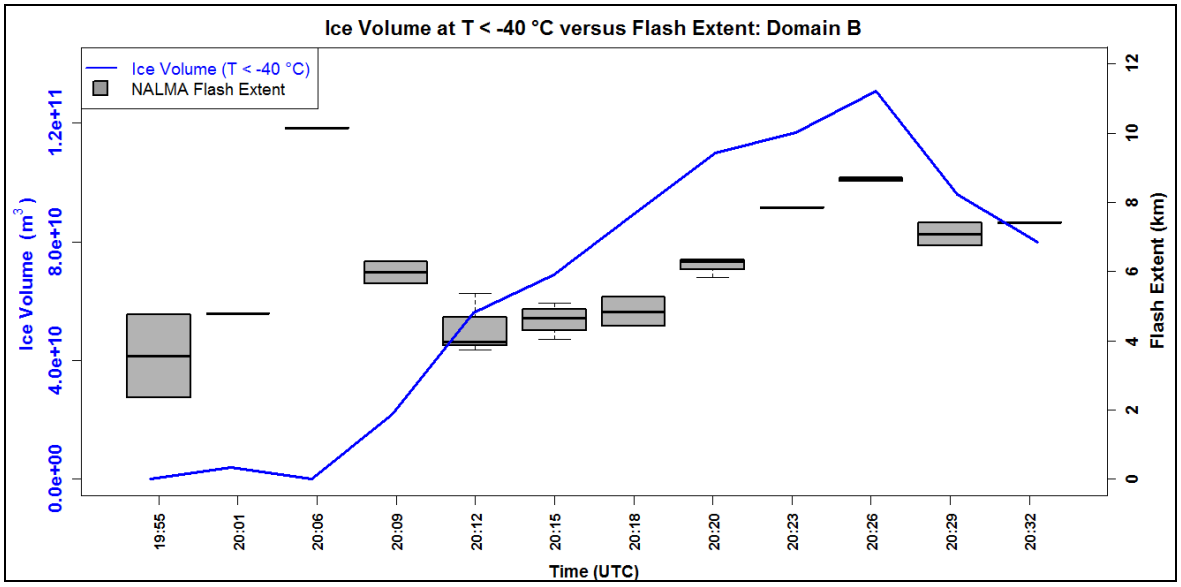

FIGURE 12: Same as Figure 11, but for domain B.

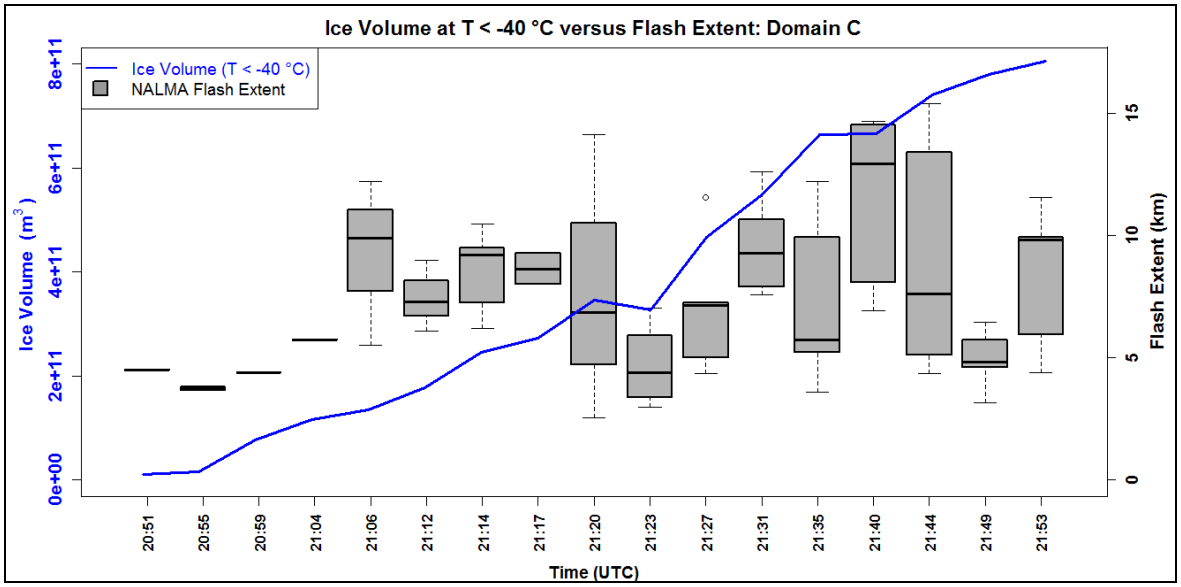

FIGURE 13: Same as Figure 11, but for domain C.

TABLE 3: Pearson Correlation Coefficient (r) when comparing the median, maximum and total flash extent per radar volume time to the ice volume aloft for Z_H > 10 dBZ at T < -40 °C

	Domain A	**Domain B**	**Domain C**	**Domain D**	**Domain E**
Median Extent with Ice Aloft	0.79	0.32	0.39	0.47	0.33
Maximum Extent with Ice Aloft	0.95	0.30	0.62	0.75	0.68
Total Extent with Ice Aloft	0.30	0.55	0.79	0.58	0.86

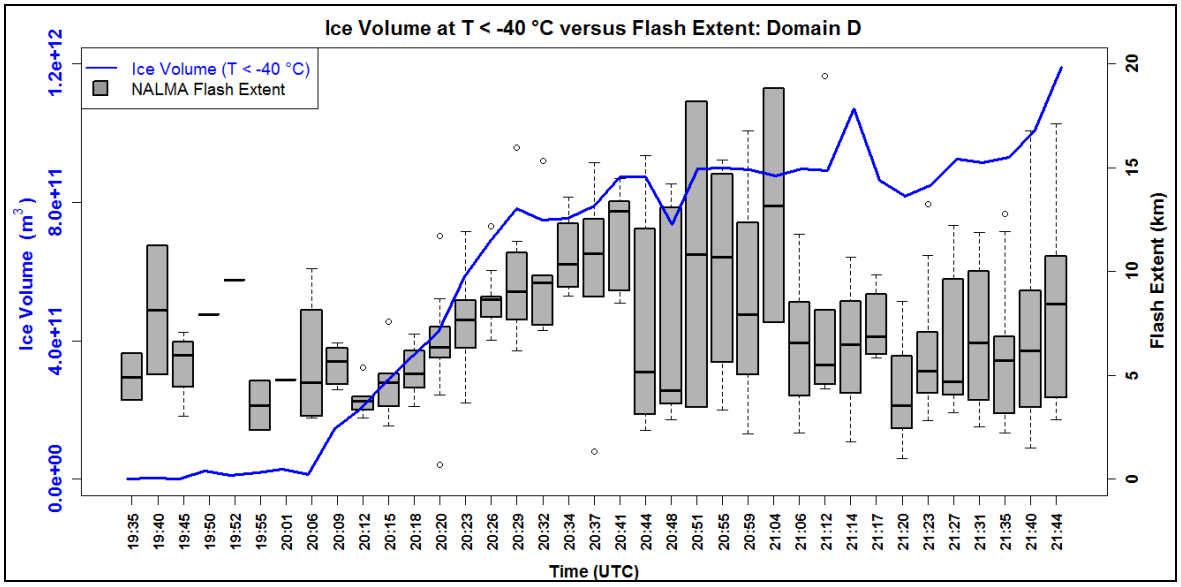

FIGURE 14: Same as Figure 11, but for domain D.

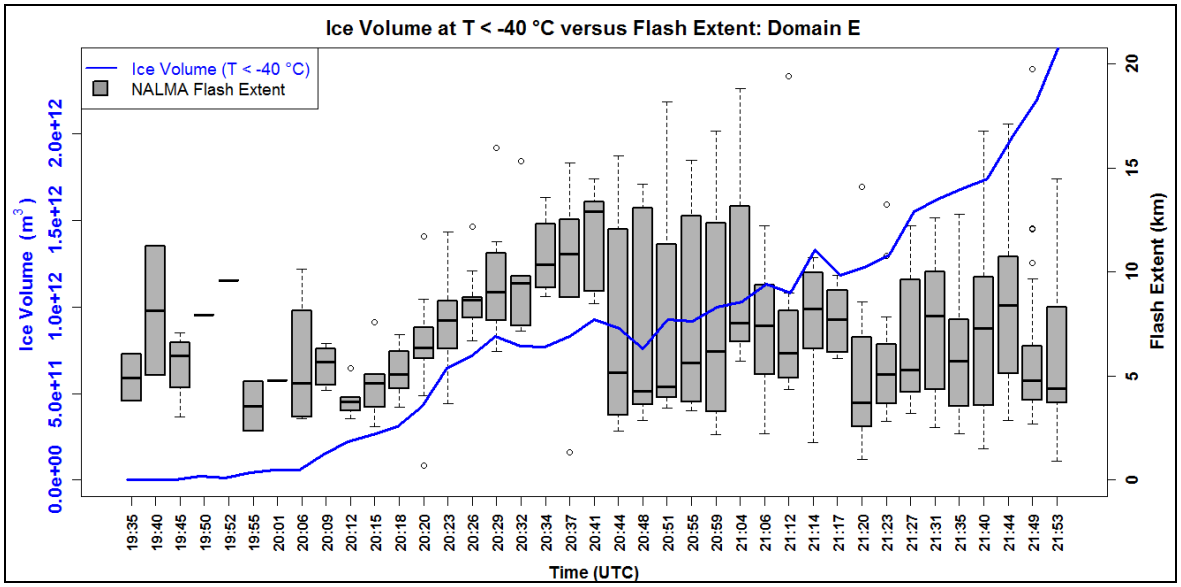

FIGURE 15: Same as Figure 11, but for domain E.

Flash Count versus total flash extent

Due to the flash extents and the spread in these extents increasing after an increase in the convective core and as the flash rates decrease, it was decided to investigate the changes in the total flash extents. These are all the flash extents for a given flash count, added together. The flash rates and associated total flash extents were binned into each minute from first flash (i.e. the flash rate is min^{-1}) for all domains (not shown); while Figure 12 shows the flash rates and associated total flash extents that were binned into the radar bin times (as was the case for Figs. 6 – 15) which is ~ 3 to 5 minutes. The reason for looking at both min^{-1} and per radar time was to learn whether or not the binning time is important, especially when it is less than 5 minutes. For the most part, the results look similar, and that is that the flash rate and total flash

extents are fairly correlated ($r \geq 0.78$), whether one bins the flashes into a per-minute bin or a radar-bin of ~ 3 to 5 minutes. However, there are some differences.

Most notably is the "raggedness" of the results when a minute bin is used (not shown); the data that is binned per radar time is more smoothed, and therefore one can more easily compare the flash rates to the total flash extents and radar products. It is also important to note that for Domain B and C, the flash rates were very low compared to the other domains (see also Table 2), with a maximum of 2 flashes min^{-1}, leading to much more variability; whereas this variability is smoothed in Figures 16 (b and c) due to the flashes being binned over longer times. As such, Domain B has a decrease in the Pearson correlation coefficient (r) from 0.92 to 0.78 (Fig. 16b) after the data is smoothed indicating that the r value is misleading when one uses low flash rates [Wilks 2006]. For the remaining domains (A, C D and E), r either remained the same, or increased marginally (less than 0.03) once the data was smoothed over a longer time-frame (i.e. over the radar bins).

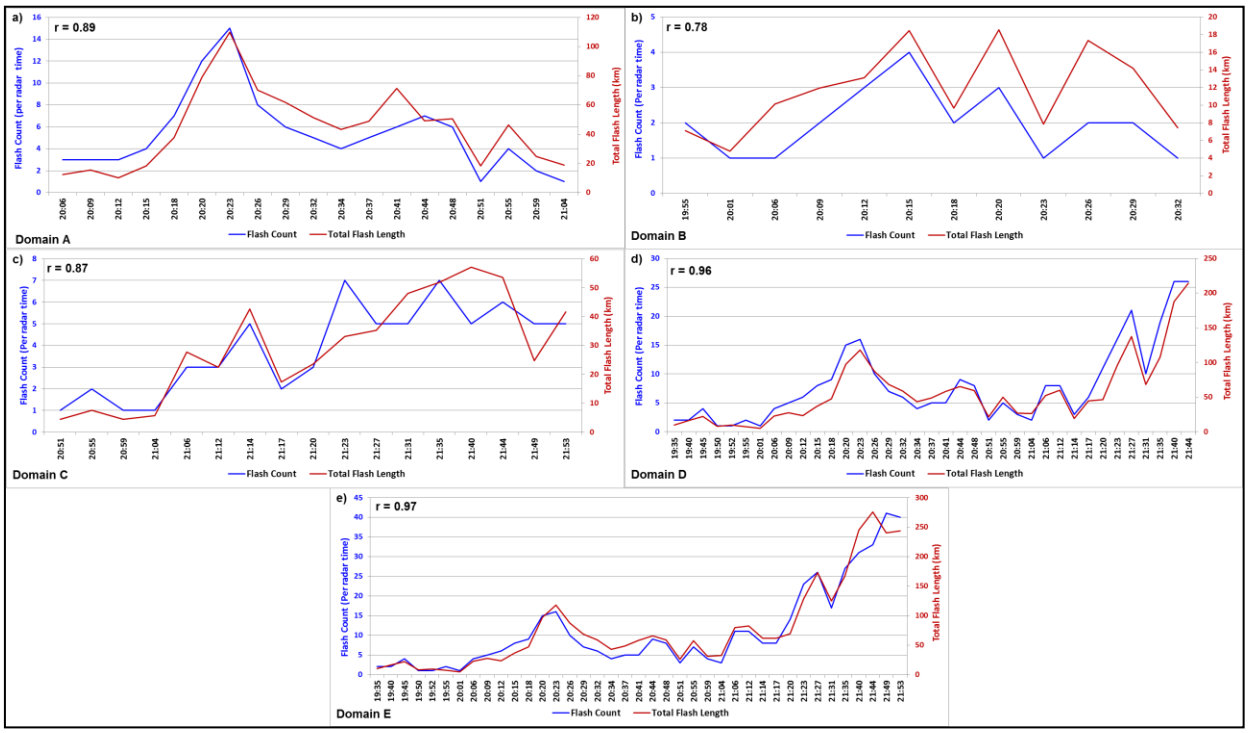

FIGURE 16: Flash rate per radar time (blue; left abscissa) compared to the total flash extent (km) for each radar time (red, right abscissa) for (a) Domain A, (b) Domain B, (c) Domain C, (d) Domain D and (e) Domain E. The Pearson Correlation Coefficient, r, is shown for each domain.

This indicates that for the most part, the flash rates and total flash extents are correlated, but it is important to note that this might not always be the case, and further analysis is needed, including looking at different types of storms and not just multi-cellular complexes. If these flash rates and total flash extents (over a certain time interval) are highly correlated for other types of storms as well, then the current LNO_X measurements where flash rates are more important and flash extents are not used, should not be influenced. However, if it is shown that these are not always correlated for other types of storms,

such as supercells and MCSs, then the flash parameterization schemes used in the calculation of LNO_X might have to be adjusted to incorporate either total flash extents or flash extents per flash.

Flash extent per flash type

Another important flash parameter that is used in LNOx estimations is the flash type. As stated above, many LNO_X modeling studies distinguish between IC and CG flashes and state that CG flashes produce more NO_X than IC flashes. However, no such study exists on which type of lightning has a larger flash extent. If the flash length/extent is indeed important in the calculation of LNO_X, as suggested by Wang et al. [1998] and Barthe and Barth [2008], then it is important to analyze the flash extents between IC and CG flashes. In addition, the IC-CG Hybrid Flashes (as explained earlier, these flashes are essentially a hybrid between IC and CG flashes and is when the VHF sources occur at a high altitude [~ > 6 km] and has either a positive or negative NLDN CG event at the same location and time interval) will also be analyzed. For this IC, CG and IC-CG Hybrid analysis, it is important to note that only specifically classified flashes were used (refer to Table 1) and therefore no "unclassified" flashes were used in order to keep the data "pure" and not bias the results. The results of this analysis is seen in Figure 17, which shows the average flash extents of the IC, CG and IC-CG Hybrid flashes for each of the 5 domains (A – E).

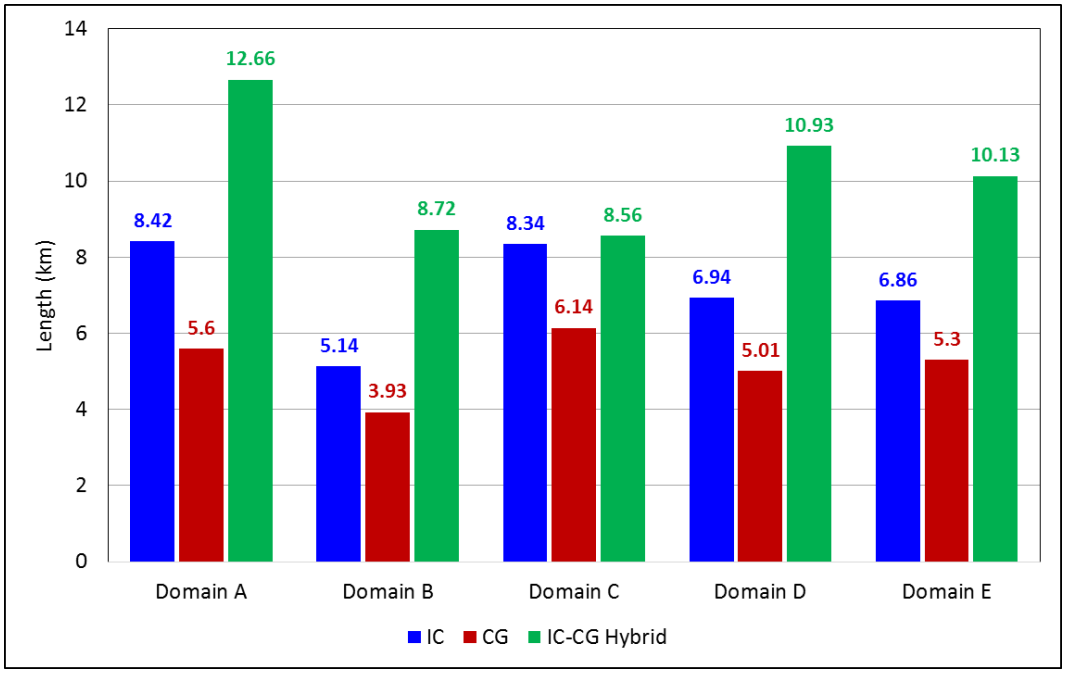

FIGURE 17: Average flash length (km) per storm domain per flash type as explained in Table 1. The average flash length per flash type is shown and color-coded according to the flash type (i.e. IC is blue, CG is red and IC-CG Hybrid is green).

The figure shows that IC-CG Hybrid flashes (~10.2 km) have areal extents roughly double that of CG flashes (~5.2 km); while pure IC flashes (~7.1 km) have a larger areal extent than pure CG flashes. These averages were obtained by first calculating the flash extent per flash over the entire time interval as

indicated in Table 2 and then obtaining the average value for each domain. The fact that IC-CG Hybrid flash extents are roughly double that of pure CG flashes and that pure IC flashes have larger extents than pure CG flashes is also true for all domains, whether one looks at a small multi-cellular complex, or a larger domain spanning over 10,000 km^2. Whether this is *always* the case for *all types* of storms, such as supercells and MCSs (and others), remains to be seen. It is imperative however to do the same analysis over other types of storms, because if these flash extents per flash types are applicable to other storms, it should have a major impact on how LNO_X modeling is done globally. It is also clearly important to make the additional distinction between pure CG flashes and IC-CG Hybrid flashes, as the IC-CG Hybrid flashes undoubtedly have much larger areal extents than pure CG flashes (shown in Fig. 17). Future work will include this same analysis over a wide variety of storms, and also include looking at the time-rate of change of these specific flash types in order to learn whether the flash extents per flash type also vary over time.

In addition, it is also important to verify whether or not the convex hull *volume* will show the same results, or whether the results will change. Currently, the convex hull *area* used in this analysis, just takes into account the horizontal extent of a flash and not the vertical extent (direction of vertical propagation) when calculating the area [Bruning and MacGorman 2013]. Hence, it is important to calculate the convex hull *volume* while the length scale is then the cube root of the volume, thereby taking the vertical propagation of the flash into account.

CONCLUSIONS

Analysis of flash extent over five different domains containing multicellular convective complexes observed during DC3 over NA demonstrated that flash extents and flash rates were generally opposed as observed by Bruning and MacGorman [2013] for supercell storms. More specifically, the presence of smaller flashes was associated with peaks in the convective pulses (seen by increases in flash rates) while larger flashes seemed to be associated with lulls in the convective pulses (seen by decreases in flash rates). It was also shown that the total flash extents are highly correlated to the flash rates ($r \geq 0.78$) and that binning the data over the radar time period leads to smoothing of the results and trivial changes in r (except when the flash rates are low). Finally, it was shown that there is a difference in flash extent between different flash types and that IC-CG Hybrid flashes have an areal extent roughly double that of pure CG flashes; while pure IC flashes have larger areal extents than pure CG flashes.

While these results are very interesting and could have a very important impact on how LNO_X is modeled in the future, more research is needed on how these features vary between storm types, such as severe and non-severe supercells, MCSs, frontal storms, and more. In addition, whether these results will occur over differing environmental regions, such as Colorado (as compared to NA) should also be investigated. Further analysis employing the convex hull volume is also necessary in order to verify whether the above results hold. Finally, attempting to understand what kinematic and microphysical properties controls the flash extents are very important, as these could have crucial impacts on how LNO_X modelling is performed when using flash rate parameterizations. In the results presented here, the ice volumes for $Z_H > 10$ dBZ at $T < -40$ °C correlated fairly well to the flash extents, and for the most part, the flash extents increased as the ice volumes increased. However, this relationship broke down for the larger domains (i.e. Domain D and E) initially when there were smaller storms in the domain that

produced lightning, but did not develop enough vertically to form ice at T < -40 °C. Also, the variability that occurred after the mature stage was reached, thus showing an increase in the ice volume aloft while the flash extents were steadily decreasing, is an indicator that the method to calculate ice volumes aloft needs to be adjusted. More specifically, investigating Dye and Willet's [2007] finding that horizontally extensive electric field magnitudes > 10 kVm^{-1} existed in long-lived anvils where Z_H > 20 dBZ, and applying this to a variety of storm types while analyzing the convex hull area and volumes relative to these reflectivity values, are imperative and will be incorporated in future analysis of this type.

ACKNOWLEDGMENTS

We wish to thank Dr. Bradley Smull (Program Director, NSF PDM) and recognize funding from the National Science Foundation`s Physical and Dynamical Meteorology (NDF PDM) Program (AGS-1063573), which has supported the DC3 field experiment and associated research. We also wish to thank the many, many people who made the collection of DC3 observations possible.

REFERENCES

Bain, A.L. 2013: Polarimetric Doppler radar and electrical observations of deep moist convection across northern Alabama during the Deep Convective Clouds and Chemistry Experiment, M.S. thesis, 148 pp., Dept. of Atmospheric Sciences, University of Alabama in Huntsville.

Bain, A.L., R. Matthee, and L.D. Carey, 2013 : Polarimetric radar and electrical observations of deep moist convection across northern Alabama during the DC3 Experiment, Paper presented at *AMS 36th Conference on Radar Meteorology*, September 16-20, Breckenridge, CO, USA.

Barth, M. C., W. Brune, C. Cantrell, S. A. Rutledge, J. H. Crawford, F. Flocke, and H. Huntrieser, 2013: Overview of the Deep Convective Clouds and Chemistry Experiment, paper J7.1 presented at the *AMS 6th Conf. on the Meteorol. Appl. of Lightning Data*, Austin, Texas.

Barthe, C., J.-P. Pinty, and C. Mari, 2007: Lightning-produced NO_X in an explicit electrical scheme: a STERAO case study, *J. Geophys., Res*., **112**, D04302.

Barthe, C. and M.C. Barth, 2008: Evaluation of a new lightning-produced NO_X parameterization for cloud resolving models and its associated uncertainties, *Atmos. Chem. Phys*., **8**, 4691 – 4710.

Bringi, V.N., T.D. Keenan, V. Chandrasekar, 2001: Correcting C-Band radar Reflectivity and Differential Reflectivity Data for Rain Attenuation: A Self-Consistent Method With Constraints. *IEEE Transc. on Geo. and Rem. Sens*, **39**, 1906-1915.

Bruning, E. C. and D. R. MacGorman, 2013: Theory and observations of controls on lightning flash size spectra, J. Atmos. Sci., 70, 4012-4029.

Calhoun, K.M., D.R. MacGorman, C.L. Ziegler, M.I. Biggerstaff, 2013: Evolution of lightning activity and storm charge relative to dual-doppler analysis of a high-precipitation supercell storm, *Mon. Wea. Rev*., **141**, 2199 – 2223.

Carey, L.D., W. J. Koshak, H. S. Peterson, R. Matthee, A. L. Bain, 2013: An investigation of the kinematic and microphysical control of lightning rate, extent and NOx production using DC3 observations and the NASA Lightning Nitrogen Oxides Model (LNOM), Abstract AE31A-03, Paper presented at *American Geophysical Union Fall Meeting*, December 9-13, San Francisco, USA.

Carey, L.D., A.L. Bain and R. Matthee, 2014: Kinematic and Microphysical Control of Lightning in Multicell

Convection over Alabama during DC3, Paper presented at *23rd International Lightning Detection Conference and 5th International Lightning Meteorology Conference*, 18 - 21 March, Tucson, Arizona, USA.

Carey, L.D., M.J. Murphy, T.L. McCormick and N.W.S. Demetriades, 2005: Lightning location relative to storm structure in a leading-line, trailing-stratiform mesoscale convective system, *J. Geophys. Res.*, **110**, D03105.

Carey, L.D., W.A. Peterson, and S.A. Rutledge, 2003: Evolution of cloud–to–ground lightning and storm structure in the Spencer, South Dakota, tornadic supercell of 30 May 1998, *Monthly Weather Review*, **131**, 1811 – 1831.

Carey, L.D. and S.A. Rutledge, 1996: A multiparameter radar case study of the microphysical and kinematic evolution of a lightning producing storm, *Meteorology and Atmospheric Physics*, **59**, 33 – 64.

Carey, L.D. and S.A. Rutledge, 2000: The relationship between precipitation and lightning in tropical island convection: a c–band polarimetric radar study, *Monthly Weather Review*, **128**, 2687 – 2710.

Cressman, G.P., 1959: An Operational Objective Analysis System. *Mon. Wea. Rev.*, **87**, 367-374.

DeCaria, A.J., K.E. Pickering, G.L. Stenchikov, J.R. Scala, J.L. Stith, J.E. Dye, B.A. Ridley and P. Laroche, 2000 : A cloud-scale model study of lightning-generated NOX in an individual thunderstorm during STERAO-A, *J. Geophys. Res.*, **105**, 11601 – 11616.

DeCaria, A.J., K.E. Pickering, G.L. Stenchikov, and L.E. Ott, 2005 : Lightning-generated NOX and its impact on tropospheric ozone production : A three-dimensional modeling study of a Stratosphere-Troposphere Experiment : Radiation, Aerosols and Ozone (STERAO-A) thunderstorm, *J. Geophys. Res*. **110**, D14303.

Deierling, W., W.A. Petersen, J. Latham, S. Ellis, and H.J. Christian, 2008: The relationship between lightning activity and ice fluxes in thunderstorms, *Journal of Geophysical Research*, **113** (D15210), 1 – 20.

Dye, J.E., and coauthors, 2000 : An overview of the Stratospheric-Tropospheric Experiment : Radiation, Aersolos, and Ozone (STERAO)-Deep Convection experiment with results for the July 10, 1996 storm, *J. Geophys. Res*., **105**, 10023 – 10045.

Dye, J.E. and J.C. Willett, 2007 : Observed enhancement of reflectivity and the electric field in long-lived Florida anvils, *Mon. Wea. Rev*., **135**, 3362 – 3380.

Ely, B.L., R.E. Orville, L.D. Carey and C.L. Hodapp, 2008: Evolution of total lightning structure in a leading-line, trailing stratiform mesoscale convective system over Houston, Texas, *J. Geoph. Res*., **113**, D08114.

Goodman S.J, R. Blakeslee, H. Christian, W. Koshak, J. Bailey, J. Hall, E. McCaul, D. Buechler, C. Darden, J. Burks, T. Bradshaw, P. Gatlin, 2005: The North Alabama Lightning Mapping Array: Recent severe storm observations and future prospects. *Atmos. Res*., **76**, 423-437.

Hodapp, C.L., L.D. Carey and R.E. Orville, 2008: Evolution of radar reflectivity and total lightning characteristics of the 21 April 2006 mesoscale convective system over Texas, *Atmos. Res*., **89**, 113 – 137.

Hondl, K.D. and M.D. Eilts, 1994: Doppler radar signatures of developing thunderstorms and their potential to indicate the onset of cloud–to–ground lightning, *Monthly Weather Review*, **122**, 1818 – 1836.

Koshak, K., H. Peterson, A. Biazar, M. Khan and L. Wang, 2014: The NASA Lightning oxides model (LNOM): application to air quality modeling, *Atmos. Res*., **135 – 136**, 363 – 369.

Lang, T.J., S.A. Cummer, S.A. Rutledge and W.A. Lyons, 2013 : The meteorology of negative cloud-to-ground lightning strokes with large moment changes : Implications for negative sprites, *J. Geophys. Res. Atm.*, **118**, 1 – 11.

Lu, G., S. A. Cummer, R. J. Blakeslee, S. Weiss, and W. H. Beasley; 2012: Lightning morphology and impulse charge moment change of high peak current negative strokes, *J. Geophys. Res*., **117**, D04212.

Lund, N.R., D.R. MacGorman, T.J. Schuur, M.I. Biggerstaff, and W.D. Rust, 2009: Relationship between lightning

location and polarimetric radar signatures in a small mesoscale convective system, *Monthly Weather Review*, **137**, 4151 – 4170.

Matthee, R., L.D. Carey, and A.L. Bain, 2013: Storm physics and lightning properties over Northern Alabama during DC3, Abstract AE33B-0342, Poster presented at *American Geophysical Union Fall Meeting*, December 9-13, San Francisco, USA.

Mohr, C.G., L.J. Miller, R.L. Vaughn, and H.W. Frank, 1986: The merger of mesoscale datasets into a common Cartesian format for efficient and systematic analysis, *Journal of Atmospheric and Oceanic Technology*, **3**, 143 – 161.

Ott, L.E., K.E. Pickering, G. Stenchikov, H. Huntrieser, and U. Schumann, 2007 : Effects of lightning NOX production during the 21 July European Lightning Nitrogen Oxides Project storm studied with a three-dimensional cloud-scale chemical transport model, *J. Geophys. Res.*, **112**, D05307.

Petersen, W. A., K. Knupp, J. Walters, W. Deierling, M. Gauthier, B. Dolan, J. P. Dice, D. Satterfield, C. Davis, R. Blakeslee, S. Goodman, S. Podgorny, J. Hall5, M. Budge, A. Wooten, 2005: The UAH-NSSTC/WHNT ARMOR C-band Dual-Polarimetric Radar: A unique collaboration in research, education and technology transfer, paper presented at *AMS 32nd Radar Meteorology Conference*, Albuquerque, New Mexico, USA.

Pickering, K.E., Y. Wang, W.K. Tao, C. Price, and J.-F. Müller, 1998: Vertical distributions of lightning NO_X for use in regional and global chemical transport models, *J. Geophys. Res.*, **103**, 31203 – 31216.

Price, C., J. Penner, and M. Prather, 1997 : NOX from lightning. 1. Global distribution based on lightning physics, *J. Geophys. Res.*, **102**, 5929 – 5941.

Qie, X., Z. Wang, D. Wang and M. Liu, 2013 : Characteristics of positive cloud-to-ground lightning in Da Hinggan Ling forest region at relatively high latitude, northeastern China, *J. Geophys. Res. Atm.*, **118**, 13393 – 13404.

Schumann, U. and H. Huntrieser, 2007: The global lightning-induced nitrogen oxides source, *Atmos. Chem. Phys.*, **7**, 3823 – 3907.

Straka, J.M., D.S. Zrnić, and A.V. Ryzhkov, 2000: Bulk hydrometeor classification and quantification using polarimetric radar data: synthesis of relations, *Journal of Applied Meteorology*, **39**, 1341 – 1372.

Thomas, R., P. Krehbiel, W. Rison, J. Harlin, T. Hamlin and N. Campbell, 2003 : The LMA flash algorithm, *Proc. 12th Int. Conf. On Atmospheric Electricity*, Versailles, France, International Commission on Atmospheric Electricity, 655 – 656.

Wang, J.–J., and L.D. Carey, 2005: The development and structure of an oceanic squall–line system during the South China sea monsoon experiment, *Monthly Weather Review*, **133**, 1544 – 1561.

Wang, Y., A.W. DeSilva, and G.C. Goldenbaum, 1998: Nitric oxide production by simulated lightning: Dependence on current, energy and pressure, *J. Geophys. Res.*, **103 (D15)**, 19149 – 19159.

Wiens, K. C., S.A. Rutledge, and S.A. Tessendorf, 2005: The 29 June 2000 Supercell observed during STEPS. Part II: Lightning and Charge Structure. *J. Atmos. Sci.*, **62**, 4151-4177.

Wilks, D.S., 2006: *Statistical Methods in the Atmospheric Sciences*, 2nd Edition, Academic Press, Oxford, pp. 627.

Zang, X., J.H. Helsdon, and R.D. Farley, 2003: Numerical modeling of lightning-produced NO_X using an explicit lightning scheme: 2. Three-dimensional simulation and expanded chemistry, *J. Geophys. Res.*, **108 (D18)**, A21 – A37.